VACUUM SYSTEMS OF ELECTRON STORAGE RINGS

D. Krämer
BESSY, Berlin, Germany

Abstract
Designers of vacuum systems of modern high intensity electron storage rings have to carefully consider vacuum pressure effects as well as geometrical and electromagnetic constraints. This paper reviews the basic aspects of synchrotron radiation determining the dynamical vacuum pressure in the presence of beam. The processes of thermal and photon induced desorption are discussed so that a proper estimate of the gas load can be made. The relevant vacuum dependent loss mechanisms are summarised in order to calculate the beam-gas lifetime. Implicit geometrical aspects in the context of machine impedance are mentioned as they have a strong influence on beam stability.

1. INTRODUCTION

Beam lifetime and beam stability are of major importance to any storage ring and require a careful design of the vacuum system. The interaction of the stored particles with the molecules of the residual gas leads to particle losses, thus calculating the pressure to be expected is essential at the design stage.

The gas load and thus the resulting vacuum pressure is determined by thermal desorption and moreover by the dynamical gas load which is produced by synchrotron radiation falling on the chamber walls. The interaction of beam particles with the residual gas molecules, cause particle losses by elastic and inelastic scattering processes. The knowledge of these processes allows the beam-gas lifetime to be calculated. Nevertheless implicit requirements such as the chambers' impedances have to be taken into account by the designers to avoid beam instabilities caused by wake fields arising from the interaction of the beam self-field with the metallic vacuum-chamber boundaries.

2. SYNCHROTRON RADIATION ASPECTS IN ELECTRON STORAGE RINGS

It has been known for about 100 years that an accelerated "electric charge concentrated in a point" radiates energy [1]. Starting from Maxwell's equation of 1873, Liénard [1] and Larmor [2] worked out the power that is emitted by a moving charged particle at non-relativistic velocities. This energy loss of accelerated particles was of concern already at the early betatrons. [3, 4], but it took until 1947 until Elder and co-workers [5] saw a "small spot of brilliant white light" in the visible spectrum, radiated from the 70 MeV electron beam of their synchrotron. That's why this electromagnetic radiation is still called "Synchrotron Radiation" (SR).

Since the energy and the stored intensities of electron beams in storage rings have been raised to much higher values, SR has an enormous impact on the design of electron-ring accelerators. The power of the SR beams that hit the vacuum chamber in modern storage-ring-based synchrotron radiation light sources or B-meson factories can be as high as $kW \cdot m^{-1}$ causing thermal problems as well as severe desorption.

2.1 Basic properties of synchrotron radiation

Amongst earlier articles, Schwinger published the theory of synchrotron radiation in 1949 [6]. A more modern derivation of the theory is found in Ref. [7], where an analytical expression of the spectral and angular distribution of SR is given in terms of modified Bessel-functions $K_{n/m}$. For recent review articles with connection to accelerators see also Refs. [8, 9].

The relativistic γ-parameter of an electron with total energy E is defined as

$$\gamma = \frac{E}{m_e c^2}$$

with c the speed of light and m_e = 511 keV/c^2 the electron rest mass. An electron (with charge e) moving in a circular accelerator will radiate a total energy W per solid angle dΩ per unit frequency interval dω per turn of

$$\frac{\mathrm{d}^2 W}{\mathrm{d}\Omega\,\mathrm{d}\omega} = \frac{e^2}{16\pi^3 \varepsilon_0\, c}\,\gamma^2 \left(\frac{\omega}{\omega_c}\right)^2 \left(1+\gamma^2\Psi^2\right)^2 \left[\mathrm{K}^2_{2/3}(\xi) + \frac{\gamma^2\Psi^2}{1+\gamma^2\Psi^2}\,\mathrm{K}^2_{1/3}(\xi)\right]. \qquad (1)$$

where ε_o = 8.86·10^{-12} A·s·V^{-1}·m^{-2} is the dielectric constant and the argument of the Bessel-function ξ is

$$\xi = \frac{\omega}{\omega_c}\cdot\frac{(1+\gamma^2\,\Psi^2)^{3/2}}{2} \quad \text{with the 'critical' frequency defined as } \omega_c = \frac{3}{2}\cdot\frac{\gamma^3\,\mathrm{c}}{\rho}.$$

The terms in the square bracket of Eq. (1) describe the fact that SR is linearly polarised in the horizontal, and circularly polarised in the vertical plane. The angular divergence and thus the peak intensity of the radiated energy are functions of frequency ω and depend on the vertical observation angle ψ. Approximating the vertical divergence at the critical frequency $\omega = \omega_c$ by a Gaussian, the divergence (FWHM) is $\alpha \approx \gamma^{-1}$. So already at small electron energies, e.g. 500 MeV, where $\gamma \cong 1000$, the vertical opening angle of SR is of the order of 1 mrad. Thus SR is extremely well collimated with a very small vertical extension.

Integrating Eq. (1) over all frequencies, the total radiated energy per unit solid angle per electron per turn gives:

$$\frac{\mathrm{d}W}{\mathrm{d}\Omega} = \frac{7\,e^2\,\gamma^5}{64\,\pi\,\varepsilon_0\,\rho}\cdot\frac{1}{\left(1+\gamma^2\,\Psi^2\right)^{5/2}}\left[1+\frac{5\,\gamma^2\,\Psi^2}{7\,(1+\gamma^2\,\Psi^2)}\right]. \qquad (2)$$

This equation indicates that SR is of concern to electron rings rather than to current hadron machines; the γ^4-dependence of Eq. (2) results in a ~10^{-13} smaller amount of SR power radiated by a proton beam (at the same energy and bending radius), as the mass ratio of proton and electron mass m_p/m_e = 1836.

As energy is radiated in quanta (photons) with energies $u = h\omega/2\pi$, the distribution of the number of photons $n(u)$ emitted by a single electron to an unit energy interval Δu per second is

$$n(u)\,\Delta u = \frac{\mathrm{d}W}{\mathrm{d}\omega}\,\frac{c}{2\pi\rho}\,\frac{1}{\hbar\omega}\,\Delta\omega$$

where $\hbar$ is Planck's constant and ρ the electron's bending radius in the external magnetic field. Thus the flux of photons emitted per second by a single electron is:

$$\frac{\mathrm{d}N}{\mathrm{d}t} = \dot{\mathrm{N}} = \int n(u)\,\mathrm{d}u = \frac{5}{2\sqrt{3}}\,\frac{e^2}{4\pi\varepsilon_o\hbar}\,\frac{\gamma}{\rho}\ . \qquad (3)$$

Equation (2) in practical units of beam energy E, magnetic bending field B and circulating beam current I for the peak power density in the horizontal plane (ψ = 0) becomes

$$\frac{\mathrm{d}P}{\mathrm{d}\Omega} = 5.42\cdot E^4\,[\mathrm{GeV}]\cdot \mathrm{B}[\mathrm{T}]\cdot \mathrm{I}[\mathrm{A}] \quad \mathrm{W}\cdot\mathrm{mrad}^{-2}$$

and integrated over all vertical angles the total power radiated by the beam into the horizontal plane is:

$$\frac{\mathrm{d}P}{\mathrm{d}\theta} = 4.42 \cdot E^3\,[\mathrm{GeV}] \cdot \mathrm{B}\,[\mathrm{T}] \cdot \mathrm{I}\,[\mathrm{A}] \quad \mathrm{W} \cdot \mathrm{mrad}^{-1}\,, \tag{4}$$

while from Eq. (3) the photon flux emitted into the horizontal plane is:

$$\frac{\mathrm{d}\dot{N}}{\mathrm{d}\theta} = 1.3 \cdot 10^{17} \cdot \mathrm{E}\,[\mathrm{GeV}] \cdot \mathrm{I}\,[\mathrm{A}] \quad \mathrm{photons} \cdot \mathrm{s}^{-1} \cdot \mathrm{mrad}^{-1}\,. \tag{5}$$

The power adsorbed by the vacuum chambers and the power distribution in the accelerator depends in detail on the vacuum chamber design but is easily estimated from geometrical considerations.

Technical problems arising from too high power loads on the chamber walls are:

- heating of the chamber walls enhancing thermal desorption;
- thermal expansion of the chambers causing current-dependent deflection of chambers and elements installed in the vacuum system, which may create position shifts of lattice elements and thus intolerable beam orbit drifts;
- photon induced desorption increasing the vacuum pressure due to a current-dependent gas load affecting the beam lifetime.

3. LINEAR POWER DENSITY

Equations (4) and (5) are the power and photon flux that are emitted by the beam whenever electrons are deflected in a magnetic field. In a dipole field B = constant, the beam is bent in a circle with constant bending radius ρ. The power of SR, as well as the photon flux, are emitted tangentially to the beam path and will hit the vacuum chamber wall. Due to the small vertical dimension of the photon beam it is useful to define the 'linear power density' $p_{\mathrm{lin}} = \mathrm{d}P/\mathrm{d}L$ as the vertically integrated power per unit length of chamber wall, Fig. 1. Taking small differences rather than differentials, the power radiated by the electron beam in a small angle segment $\Delta\theta$ is dissipated along a distance ΔL on the chamber walls. By this the linear power density distribution along the whole machine is:

$$p_{lin} = \frac{\mathrm{d}P}{\mathrm{d}L} \cong \frac{\mathrm{d}P}{\mathrm{d}\theta}\frac{\Delta\theta}{\Delta \mathrm{L}}.$$

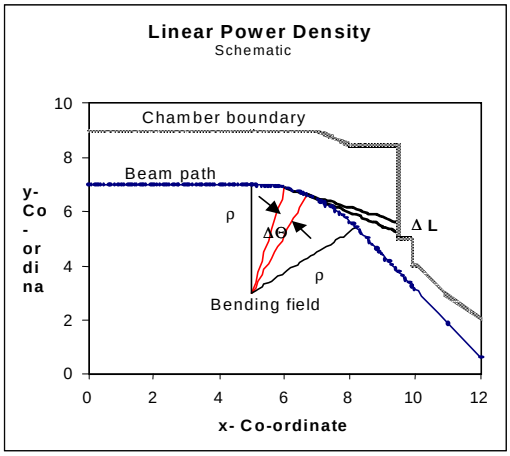

Fig. 1 Schematic of the concept of linear power density. The power P radiated in the angle segment $\Delta\theta$ is spread over a distance ΔL at the vacuum system boundary. The linear power density p_{lin} is the power absorbed by the chamber wall per unit length.

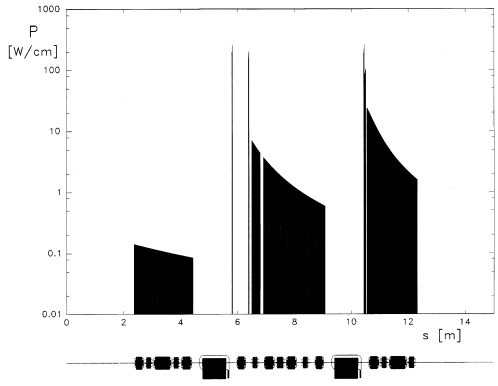

Fig. 2 Linear power density distribution along a unit cell of the BESSY II synchrotron light source (1/16 of the ring circumference). Near the exit of the bending magnets the power density is as high as 250 W/cm. Input data: energy 1.9 GeV, stored current 500 mA, bending field 1.45 T. The minor contribution of multipole magnets is neglected in the calculation. The magnetic lattice of the ring is sketched in the lower part of the graph.

It is obvious that by simple means, e.g. avoiding surfaces perpendicular to the incoming

photon beam, the peak power density can be decreased by distributing the power over a larger distance ΔL. Figure 2 shows a calculation of the linear power density for the 1.9 GeV BESSY II SR light source. For a stored current of 500 mA the linear power density ranges from 250 W/cm near the exit of the bending magnets to less than 1 W/cm in the straight sections. Especially at the location of high power load, a careful analysis of the expected temperatures and thermal deflection of components has to be done (using standard FEM programs) to avoid damage to the hardware components.

The same concept is used to derive the linear photon flux density n_{lin} = d(dN/dt)/·dL [photons·s^{-1}·cm^{-1}] on the chamber walls using Eq. (5):

$$n_{lin} = \frac{\mathrm{d}\dot{\mathrm{N}}}{\mathrm{d}\theta}\frac{\Delta\theta}{\Delta L}. \qquad (6)$$

4. THERMAL- AND PHOTON-INDUCED DESORPTION

For a vacuum system without beam, the gas originates from a variety of processes as permeation, diffusion, desorption/re-adsorption and the material's vapour pressure. For electron rings it is normally sufficient to consider the thermal desorption of molecules bound to the chamber-wall surfaces only. In the presence of electron beams the photon-induced desorption by synchrotron radiation gives a significant contribution to the vacuum pressure.

4.1 Thermal desorption

The surfaces of the vacuum vessels are always covered with some layers of molecules which are adsorbed at binding energies in the range of eV. In consequence continuous gas loads Q_i consisting of gas components 'i' like H_2, CH_4, H_2O, CO, CO_2 are desorbing, giving a total gas load Q_o:

$$Q_\mathrm{o} = \sum_i Q_i$$

The desorption rates q_i [mbar·l·s^{-1}·cm^{-2}], often also termed specific outgassing rate, are the gas loads per surface area A: $q_i = Q_i/A$. These rates cannot be calculated by general means, as they are a property of the material and depend on its history, e.g. the way the surfaces have been cleaned [10].

According to Frenkel's equation, the gas load Q_i depends on temperature T. Q_o is the sum of all the desorbing components i, at a surface coverage N_i [molecules·cm^{-2}] and binding energy E_i:

$$Q_\mathrm{o} \propto \sum_i N_i \, e^{-\frac{E_i}{\mathrm{k}T}} .$$

Baking the vacuum system increases the temperature T and enhances desorption. For clean stainless steel-samples specific outgassing rates of 10^{-12} mbar·l·s^{-1}·cm^{-2} are achieved routinely after in-situ bakeout at ~300^0 C. In unbaked systems the outgassing rate is typically a factor of 5 to 10 higher.

Let us assume that the specific outgassing rate as function of time $q_i(t)$ is proportional to the total amount of gas $q_{o,i}$ adsorbed on the surface

$$q_\mathrm{i}(t) = -\,\mathrm{d}q_{o,\mathrm{i}}/\mathrm{d}t \, .$$

When the surface coverage is considered to change by desorption only

$$N(t) = \sum [N_i(t = 0) - (\int q_i \, \mathrm{d}t)]$$

the gas load Q_i will decrease exponentially with respect to time at a characteristic time-constant τ_i for each gas species of a Frenkel type relation:

$$\tau_i = \tau_o \exp(-E_\mathrm{i}/\mathrm{k}T) \, .$$

When assuming that for a baked and an unbaked system the binding energies are the same (since the relative composition of adsorbates stays unchanged – which definitely is an over-simplification) it takes a time of approximately $2.3\tau_b$ for an unbaked system to arrive the gas load Q_b of a baked one (and thus at a vacuum pressure $P_b = Q_b/S$). Here τ_b is the time it needs to reduce Q_o by a factor of $1/e$ in the baked system. So, for a thermal desorption dominated vacuum system bake-out is useful to achieve low pressures in a short time.

4.2 Photon-induced desorption

In the presence of SR the balance of outgassing is significantly changed. Synchrotron radiation on one hand increases the temperature of the vacuum chamber, therefore increasing thermal desorption. On the other hand the SR photons hitting the vacuum chamber walls create photoelectrons which scatter on the walls, causing adsorbed molecules to desorb [11]. Thus the total gas load has to be considered as the sum of thermal and photon induced desorption

$$Q = Q_0 + \eta \dot{N} k,$$

where Q_0 is the thermal gas load and η the desorption yield, e.g. the number of molecules released per incident photon, k is the conversion factor from molecules to Torr l ($k = 3.1 \cdot 10^{-20}$ Torr·l·molecules^{-1} at 25 °C) and dN/dt the photon flux. According to Eq. (6) the photon flux is a function of position in the machine.

A variety of measurements to determine the desorption yield η have been published, [12–14]. The desorption yield η is decreasing with time or, to be more precise, with the accumulated photon flux, also named "photon dose". The desorping molecules follow a dependence:

$$\eta = \eta_0 D^{-\alpha},$$

where η_o is the initial desorption rate of the order of 10^{-2} [molecules·photon^{-1}] for most gas species such as H_2, CO and CO_2 from standard materials such as stainless steel, copper and aluminium. It is obvious that η_o is a quantity that depends on the cleaning procedure. It also depends on the history of the material. α determines the dependence on photon dose D (e.g. the integrated photon flux [photons] or integrated electron current with respect to time [A·h] using Eqs. (4) and (5), respectively). Typical values of α are 0.8 to 1.2. Water, which is loosely bound by van der Waals forces, behaves somewhat differently in this context [14].

Figure 3 displays a typical measurement result of the desorption yield for an OFHC-copper surface, [15]. Starting at $\eta_o \cong 10^{-2}$ at a dose of some 10^{20} photons, the yield is rapidly decreases to values below 10^{-6} after a dose of 10^{24} photons, equivalent to an integrated beam current of ~50Ah — as 10^{18} photons·s^{-1} were hitting the sample. This well-known effect, often called "beam scrubbing", is a powerful cleaning method for vacuum surfaces in electron machines.

Calculation of the desorption distribution thus has to reflect the desorped gas load $Q(x,\eta(D))$ which is dependent on the photon flux at location x as well as on the desorption yield which itself depends on the accumulated beam dose D. In order to determine the mean gas pressure, we have to decide on the pumping scheme, the location of pumps and their pumping speed to derive the pressure distribution.

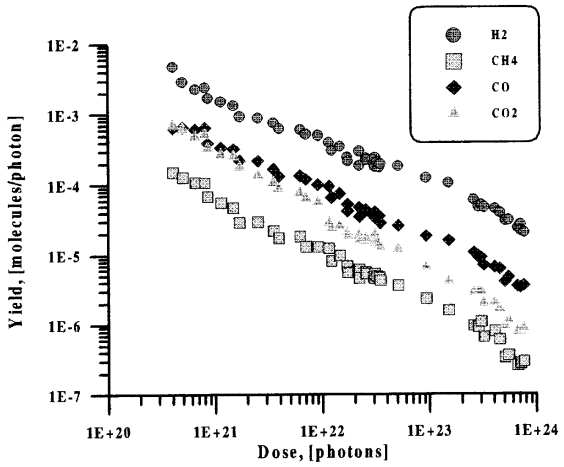

Fig. 3 Desoprtion yield vs. integrated photon dose, from Ref. [15].

5. PUMPING SCHEME & PRESSURE DISTRIBUTION

The magnetic elements of the accelerator set important geometrical boundaries to the layout of the vacuum system. The available apertures in the multipole magnets determine the cross section of the chambers. At the same time the flexibility for optimised positioning of vacuum pumps is limited by the presence of magnets and other elements. Thus, there is no simple way to optimise the vacuum system. Nevertheless one can derive a simple model of the vacuum system [10,16] to obtain a rough insight into the performance of the pumping system. As, indeed, major parts of the vacuum chambers do not change their shape, we consider a beam tube of constant elliptical cross section with pumps at constant distance L from each other. The gas flow Q [mbar·l·s^{-1}] gives rise to a pressure difference dP due to the specific conductance w [m·l·s^{-1}] of the pipe. Along the direction x of the pipe in linear approximation the gas load is

$$Q(x) = - \mathrm{w} \frac{\mathrm{d}P}{\mathrm{d}x} \ .$$

Assuming that the specific gas load q [mbar·l s^{-1}·m^{-2}] per specific surface area A [m] stays constant and the total surface of the pipe of length L is $F = AL$ [m^2], then

$$\frac{\mathrm{d}Q}{\mathrm{d}x} = Aq \ .$$

Combining the two equations gives:

$$w \frac{\mathrm{d}^2 P}{\mathrm{d}x^2} = - Aq \ . \qquad (7)$$

With the boundary conditions that the pressure is equal to AqL/S_o at the location of vacuum pumps with pumping speed S_o and that due to symmetry of the problem there is a maximum at $x = L/2$:

$$\frac{\mathrm{d}P}{\mathrm{d}x}\Big|_{x=L/2} = 0 \, ,$$

a parabolic pressure dependence follows with the average pressure:

$$\langle P \rangle = Aq \left(\frac{L^2}{12w} + \frac{L}{S_\mathrm{o}} \right) .$$

For an elliptical pipe of length L [cm] and semi-axes a [cm] and b [cm], the conductance $C = w/L$ [l· s^{-1}] for a gas molecule of mass M [amu] at temperature T [K] is given by the relation 10]:

$$C = 431 \cdot \left[\frac{a^2 \, b^2}{L} \right] \cdot \frac{1}{\sqrt{a^2 + b^2}} \cdot \sqrt{\frac{T}{M}} \qquad \mathrm{l \cdot s^{-1}}$$

Defining an effective pumping speed S_{eff}, the average pressure in the section is given by:

$$\langle P \rangle = \frac{AqL}{S_{\mathrm{eff}}}$$

with

$$S_{\mathrm{eff}} = \left(\frac{L}{12w} + \frac{1}{S_\mathrm{o}} \right)^{-1}$$

For conductance limited vacuum chambers as in the straight sections of the BESSY II storage ring the specific conductance is w = 20 m·l·s^{-1} for N_2 (M = 28). The effective pumping speed as function of distance L and pumping speed S_o is plotted in Fig. 4. The graph immediately shows that

the optimum solution is to place as many small pumps as closely together as possible when lumped pumps are used. Irrespective of the pumping speed of the pumps, the maximum effective pumping speed is limited to12w/L. Realistic distances L are about 2 to 3 m demanding pumps of typically less than 60 l/s pumping speed, yielding $S_{eff} \approx 20$ l/s. On the other hand the effectiveness of linearly distributed pumps all along the machine circumference is obvious as L approaches zero, in this concept the maximum pumping speed S_o is available at the vacuum chamber.

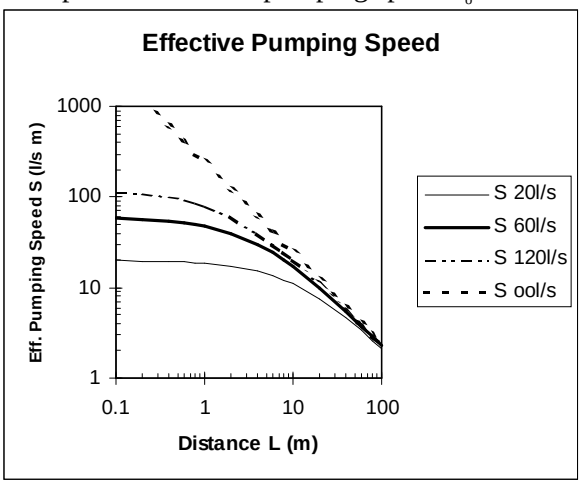

Fig. 4 Effective pumping speed of a conductance limited chamber (w = 20 m·l·s^{-1}) as function of distance L. The curves are for different values of the pumping speed S_o (20, 60, 120 l·s^{-1} and infinite pumping speed).

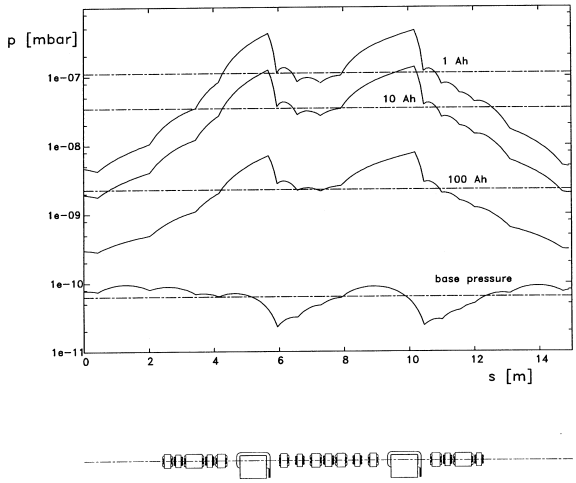

Fig. 5 Pressure distribution of a 1.9 GeV, 500 mA beam in the BESSY II storage ring as expected after accumulation of various beam doses (1, 10 and 100 A·h) as well as the base pressure without beam. The magnetic lattice of BESSY II is sketched to scale (lower part).

In a more realistic model the assumption of constant outgassing rate has to be replaced by the position dependent $q(x)$, while the varying conductances $w(x)$ have to be considered correctly. Many different computer codes have been developed to evaluate the problem Eq. (7), ranging from spreadsheet-based macros [17], up to Monte-Carlo simulations [18, 19]. Thus the pressure profile can be approximated piecewise and/or evaluated directly taking into account the dose-dependent desorption rates. Figure 5 shows a calculation that was performed for the BESSY II storage ring. The pressure distribution is plotted for different desorption conditions (accumulated doses of 1, 10 and 100 A·h) and for thermal outgassing, i.e. without beam. To achieve the design pressure of $<P> = 10^{-9}$ mbar, an integrated dose of ~ 200 A·h is required.

6. SINGLE-PARTICLE LOSS MECHANISMS

Once the vacuum pressure and the gas composition are known, scattering of the stored electrons with residual gas molecules will cause particle losses from which we will calculate the beam-gas lifetime. As the beam particles are considered to be independent from each other, beam-gas interactions are considered as incoherent effects that are treated statistically.

There are two different interactions to consider:

- Elastic scattering which leads to a transversal deflection of the beam particle. After the collision the electrons will start to perform betatron oscillations around the closed orbit. With the assumption that the beam-stay-clear aperture of the vacuum chamber is of the same size as the dynamical aperture, the particle is lost when the amplitude of the orbit oscillation exceeds the mechanical limit (mostly the vertical chamber height).
- Inelastic scattering, where a photon is emitted in the collision, changes the beam particles' energy. If the dispersive orbit exceeds the mechanical (normally the horizontal) aperture, or if the rf-acceptance limit is exceeded, the particle is lost [20, 21].

6.1 Coulomb scattering

Scattering of an idealised mono-energetic electron beam in the Coulomb field of the nucleus of a residual-gas atom of nuclear charge Z leads to an angular deflection, depending on the impact parameter b, i.e. the shortest distance between the incoming particle trajectory and the point-like target. Taking into account the screening of the Coulomb field by electrons from the target-atom which is important for particles at large b (equivalent to beam particles scattered into small angles) and modifying for the finite size of the nucleus, the differential cross section of the scattering process can be found in many text books. [7]. Integrating this cross section from the minimum angle θ_{min} for which a particle gets lost and maximum angle $\theta_{max} \cong \pi$ gives:

$$\sigma = \frac{2\pi Z^2 r_e^2}{\gamma^2} \frac{1}{\Theta_o^2}$$

As a consequence of the angle deflection θ_o the particle performs betatron oscillations with maximum amplitude

$$y_{\max} = \frac{1}{2\sin(\pi Q)} \cdot \sqrt{\beta(s)} \cdot \sqrt{\beta_i} \cdot \Theta_0 \ .$$

The particle hits the vacuum wall if $y \geq \boldsymbol{a}$. β_i and $\beta(s)$ denote the horizontal or vertical amplitude function of the ring at the location i where the scattering takes place and $\beta(s)$ somewhere in the machine, while $\boldsymbol{a}$ represents the horizontal or vertical half aperture of the chamber.

Averaging over all possible locations i (replacement of β_i by the mean beta value $<\beta>$) the cross section due to Coulomb scattering is [20, 22]:

$$\sigma_C = \frac{2\pi Z^2 r_e^2}{\gamma^2} \cdot \frac{\langle\beta\rangle \beta_{\max}}{a^2}$$

It is evident that for increasing energy this loss mechanism becomes less important.

6.2 Bremsstrahlung

Inelastic scattering of an electron off a nucleus causing bremsstrahlung leads to an energy loss of the circulating particle. The electron is lost when the energy deviation exceeds the rf acceptance ε_{rf} of the ring. The total cross section for particle loss is [22, 23]:

$$\sigma_B = \frac{4 r_e^2 Z^2 e^2}{h c} \cdot \frac{4}{3} \ln \frac{183}{Z^{1/3}} \left(\ln \frac{1}{\varepsilon_{rf}} - \frac{5}{8} \right).$$

6.3 Elastic e-e scattering

Similar to the elastic scattering of electrons off the nucleus, the beam particles also scatter with the electrons of the atoms of the residual gas. In this process the beam electrons transfer part of their energy to the gas atom. Again if the beam particles' energy loss exceeds the rf acceptance limit, the particle is lost. The total cross section for the process is [20, 21]:

$$\sigma_{el,ee} = \frac{2\pi r_e^2 Z}{\gamma} \frac{1}{\varepsilon_{rf}}$$

6.4 Inelastic e-e scattering

In inelastic scattering of the beam electrons with the electrons of the residual gas atoms, a photon is emitted, which carries away part of the electron energy. Particle loss occurs when the energy acceptance is exceeded. The loss cross section is given by [20, 21]:

$$\sigma_{inel,ee} = \frac{4\, r_e^2\, Z\, e^2}{h\, c} \cdot \frac{4}{3}\left[\ln\frac{5\gamma}{2\,\varepsilon_{\mathrm{rf}}} - 1.4\right]\cdot\left[\ln\frac{1}{\varepsilon_{\mathrm{rf}}} - \frac{5}{8}\right].$$

6.5 The beam-gas lifetime

The number of beam particles N divided by those lost per time interval -dN/dt is the 1/e-beam lifetime τ. The relative losses equal the cross section σ_i times the density of target atoms n_i (the index i corresponds to the different molecules j in the residual gas composed of k_{ij} atoms of type i with nuclear charge of Z_i). The beam travels with the speed of light c so the beam experiences a density of these target atoms per second of $\sum n_i c$. Thus the inverse beam lifetime is given by summation of the above cross sections:

$$\frac{1}{\tau} = -\frac{1}{N}\frac{\mathrm{d}N}{\mathrm{d}t} = c\sum_{j,i} k_{ij} n_i \left\{\sigma_{C,i} + \sigma_{B,i} + \sigma_{el,ee,i} + \sigma_{inel,ee,i}\right\}$$

The densities n_i of atoms i from molecules j are related to their vacuum pressure P_i via Boltzmann's constant k and the temperature T:

$$n_i = \frac{P_i}{kT}$$

At room temperature this relation in practical units is: n_i [m^{-3}] = 3.217 · 10^{22} P$_i$ [Torr].

Comparing measured and calculated beam lifetimes as a function of the circulating beam intensity show good agreement at low currents, Fig. 6. For high intensity beam, i.e. high bunch currents, especially if only a few bunches are circulating discrepancies are visible. The underlying process is scattering of electrons amongst each other inside the bunch. This effect was identified first in the small Frascati ADA ring and explained by Touschek [24]. Though the "Touschek effect" is not related to the vacuum pressure at all, it is discussed in some detail here as the horizontal aperture of the vacuum chamber is affected.

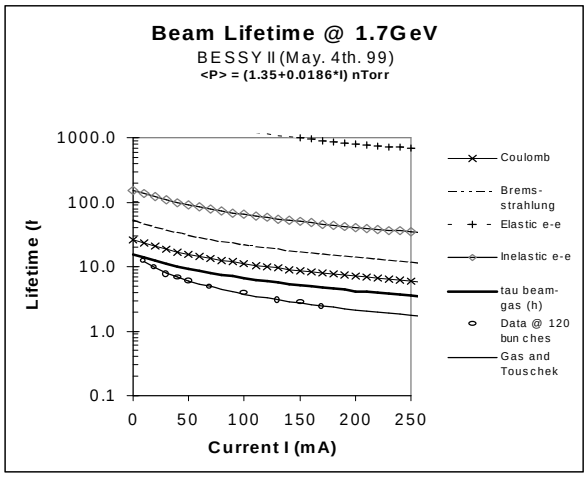

Fig. 6 Beam lifetime for the various loss mechanism as a function of the beam current in BESSY II. The calculated total beam-gas lifetime is the solid line. Solid dots represent measured data when running the current in 120 bunches. The difference of total beam-gas lifetime and measured data is due to the Touschek effect. Taking this effect into account, the measured beam lifetimes are precisely described.

6.6 Touschek effect

Low emittance synchrotron light sources as well as B-meson factories operate at high electron densities in the circulating bunches. The probability that electrons inside the same bunch scatter off each other is proportional to the particle density in the bunch. Thus current dependent particle losses further decrease beam lifetime with respect to beam-gas lifetime.

The scattering of particles within a bunch is called the Touschek effect. If the energy transfer in a collision is large enough the particle is lost if the momentum deviation exceeds the momentum acceptance of the machine. Furthermore if the scattering takes place in a dispersive region the amplitudes of the resulting horizontal betatron oscillations may exceed the geometrical vacuum chamber aperture. Touschek beam lifetime [20, 24, 26] is not related to the vacuum pressure but the vacuum chamber design may influence it via pure geometrical parameters. The inverse Touschek lifetime is given by:

$$\frac{1}{\tau} = \frac{N\, r_e^2\, c}{8\pi\, \sigma_x\, \sigma_z\, \sigma_s\, \gamma^2\, \varepsilon_{rf}^3} \cdot D(\varepsilon)$$

with

$$\varepsilon = \frac{\varepsilon_{rf}^2}{2\gamma^2} \frac{\beta_x^2}{\sigma_x}$$

for a flat beam and the *D*-function defined by

$$D(\varepsilon) = \sqrt{\varepsilon} \left\langle -\frac{3}{2} e^{-\varepsilon} + \frac{\varepsilon}{2} \int_{\varepsilon}^{\infty} \frac{\ln u}{u\, e^{u}}\, du + \frac{1}{2}(3\varepsilon - \varepsilon \ln \varepsilon + 2) \cdot \left\{ \int_{\varepsilon}^{\infty} \frac{e^{-u}}{u}\, du \right\} \right\rangle$$

It may be worthwhile to point out that the Touschek loss rate depends on the square of the number of electrons in a bunch as two electrons are involved in the collision, $dN/dt = -aN^2$. Therefore the total beam lifetime does not show an exponential decay with time t as in case of the beam-gas events. The development of current $I(t)$ with time is:

$$I(t) = \frac{I_0}{1 + I_0 \cdot a \cdot t}.$$

Depending on the machine momentum acceptance, Touschek-scattered electrons require a certain minimum beam-stay-clear aperture. As an example Fig. 7 shows the theoretical predicted Touschek lifetime at BESSY II as a function of horizontal chamber half-apertures at different momentum acceptance $\Delta p/p$ of the ring. The Monte-Carlo approach [27] is in excellent agreement with the analytical approach used in the ZAP program [28]. Thus the vacuum chamber design has to provide an aperture wide enough to allow safe operation.

Especially for low energies and high intensity storage rings one requires a more detailed analysis of multiple-small-angle Coulomb scattering (multiple Touschek scattering) [29]. The effect of intra-beam scattering has been seen in hadron and heavy-ion machines especially when phase-space-cooling techniques are used [30]. However, little time has been spent on this problem in the case of electron storage rings.

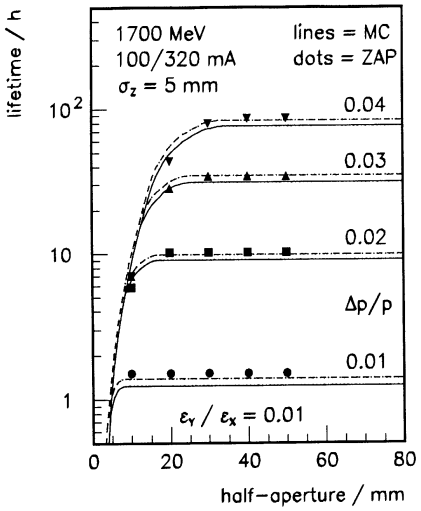

Fig. 7 Calculated Touschek lifetime for the BESSY II Synchrotron Light Source as a function of horizontal aperture and machine-momentum acceptance $\Delta p/p$. A 100 mA beam spread in 320 bunches with bunch length σ = 5 mm is assumed. The dots are lifetimes obtained using the program ZAP, the solid (dashed) lines are relativistic (non-relativistic) Monte Carlo results [27].

7. IMPLICIT REQUIREMENTS FOR THE VACUUM SYSTEM

The beam particles generate an electromagnetic "self"-field according to Maxwell's equations. The boundary conditions that are given by the geometry and electromagnetic properties of the vacuum chamber materials strongly influence the solution of the differential equations. An analytical solution of Maxwell's equation taking into account all details of an actual machine environment is definitely impossible. Nevertheless, in order to get information on instabilities generated in the beam in the presence of the electromagnetic fields, the concept of impedances was introduced. In analogy to Ohm's law, longitudinal and transversal impedances $Z_{\parallel}$ and $Z_{\perp}$ are defined [31, 32] by:

$$\left[\vec{E}_{//} + \vec{v} \times \vec{B}\right]_{//}(t,\Theta) = -\frac{1}{2\pi R}\int_{\omega=-\infty}^{\omega=\infty} Z_{//}\, S_{//}(\omega,\Theta)\, e^{j} \quad d\omega$$

and

$$\left[\vec{E} + \vec{v} \times \vec{B}\right]_{T}(t,\Theta) = -\frac{j\beta_o}{2\pi R}\int_{\omega=-\infty}^{\omega=\infty} Z_{\perp}\, S_{T}(\omega,\Theta)\, e^{j\ t}\, d\omega$$

where $S_{//}$ is the beam current and S_T the beam signal while E and B are the electrical field and induction, respectively. The impedances are considered as the origin of longitudinal and transversal beam instabilities. The impedances are complex function of frequency ω.

It is useful to distinguish between single-bunch and multi-bunch operation in the accelerator. Single bunches are affected, with respect to stability, by broadband impedances associated with short-range wake fields. The longitudinal broadband impedance may cause bunch lengthening, while the transverse impedance allows the current-dependent growth rates of instabilities (i.e. head tail and strong head tail instability) to be derived. If these growth rates are faster than the "natural" damping times due to the emission of SR, the beam will be unstable.

Similarly, when trains of bunches are circulating in the ring (multi-bunch operation), the long-range wake field and their associated longitudinal and transverse impedances can generate longitudinal and/or transverse coupled-bunch oscillations (instabilities). Only in very special cases can analytical formulae for the impedance be derived, i.e. the resistive-wall impedance of a long circular tube.

7.1 Resistive-wall impedance

The finite resistivity of the vacuum chamber is the origin of a longitudinal and transversal impedance (restive-wall impedance). For a long circular pipe of radius b the impedances are given by the analytical expressions [32, 33]:

$$Z_{\perp}(\omega) = \frac{(1-i)}{b^3}\cdot Z_o\, R\, \delta$$

and

$$\frac{Z_{//}(\omega)}{n} = \frac{(1-i)}{2\,b}\cdot Z_o\, \delta$$

with the chamber length $C = 2\pi \cdot R$ equal to the machine circumference. ρ is the resistivity of the wall material with skin depth δ given by:

$$\delta = \sqrt{\frac{2\rho}{\omega \cdot \mu_0}}\ .$$

where $\mu_o = 1.25 \cdot 10^{-6}$ Vs A^{-1} m^{-2} is the permeability of the vacuum, and $Z_0 = \mu_o \cdot c = 377\ \Omega$ the impedance of vacuum. As it is common to use Z/n rather than Z, we also will use the relation:

$$\frac{Z(\omega)}{n} = Z(\omega)\cdot\frac{\omega_o}{\omega},$$

where $\omega_o = 2 \cdot \pi \cdot f_o$ with f_o the revolution frequency of the beam in the ring.

The longitudinal impedance gives rise to a growth rate of longitudinal coupled bunch modes for a beam of n bunches and bunch-current I. If the inverse growth rate is larger than the natural damping time, the beam will be damped, otherwise the bunches start longitudinal oscillations.

Transverse coupled bunch oscillations are excited when the growth rate is smaller than the transverse radiation damping time. Fortunately – as the resistive-wall growth rate depends on chromaticity and working point of the machine – changes to the excitation of sextupole magnets in the ring or selection of a new tune can help to damp the instability. Nevertheless the b^{-3} scaling of the transverse impedance is a problem for modern SR light sources where a considerable fraction of the machine circumference is equipped with narrow vertical chambers for small gap undulators.

7.2 Impedance of the vacuum system in general

Designers of vacuum chambers are confronted with the problem of including into the machine various items such as bellows, flanges, pumping ports and tapers for changes of the chamber cross section. To evaluate their contribution to the machine impedance each item needs to be considered separately, using well known codes such as MAFIA [34] and TBCI [35]. In the time domain the wake function $W(t)$ generated by the bunch with charge distribution $I(t)$ is calculated from Maxwell's equations. The coupling impedance $Z(\omega)$ then is the complex power spectrum of the wake function normalised to the charge distribution in the frequency domain:

$$Z(\omega) = \frac{\int_{-\infty}^{\infty} W(t)\, e^{-i\omega t}\, \mathrm{d}t}{I(\omega)}.$$

Figure 8 shows an example using a Gaussian charge distribution $I(\omega) = q_1 \exp[-{}^1/_2(\omega\tau)^2]$ with the resulting wake function [36]. The geometry under consideration in the example is that of one of the 112 beam position monitors in the BESSY II storage ring. They give a significant contribution to the longitudinal impedance with a prominent resonance at $\omega = 45$ GHz.

Summing up all impedances at BESSY II gave a total longitudinal coupling impedance nearly constant over the frequency range $\omega = 0 - 140$ GHz for the BESSY II ring with $|Z/n| \cong 0.3\ \Omega$, Fig. 9.

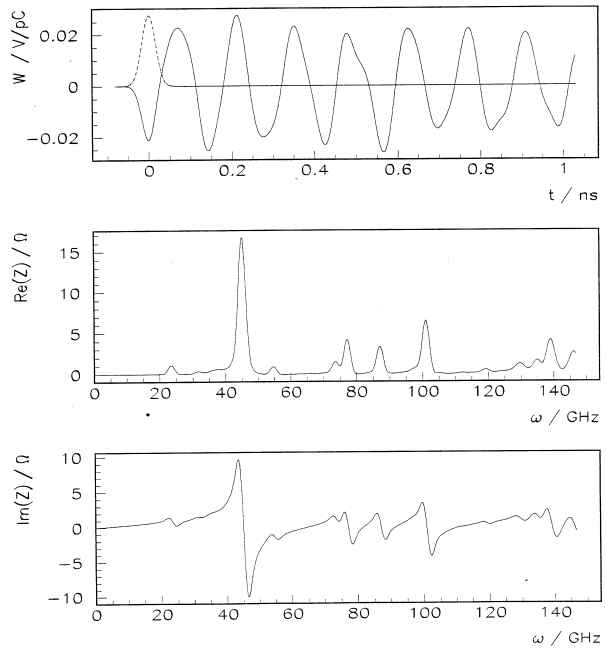

Fig. 8 Upper part: Beam charge distribution $i(t)$ and wake function $W(t)$ caused by a beam position monitor as function of time. The two lower graphs show the real and imaginary part of the longitudinal impedance [36].

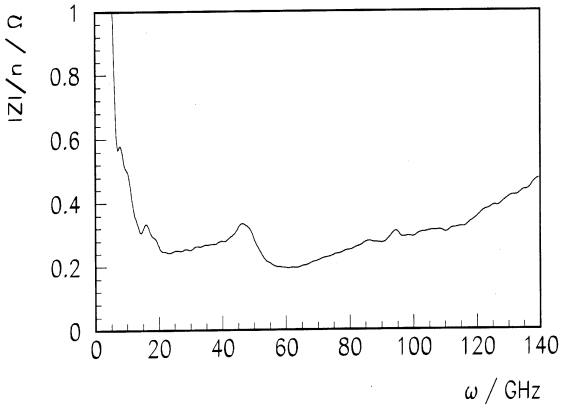

Fig. 9 Calculation of the longitudinal coupling impedance for the BESSY II storage ring [36].

8. ACCELERATOR VACUUM SYSTEMS IN ROUTINE OPERATION

Already during accelerator commissioning any error in the design and production of the vacuum hardware will show up. Effects range from incorrect vacuum gauge pressure readings, due to the sensors being installed too close to the fringe field of magnets, to enhanced desorption rates of heavy contaminants caused by inappropriate cleaning methods. Obstacles in the chambers as a result of manufacturing or cleaning errors as well as melted rf liners in bellows sometimes reduce the vacuum chamber aperture to the point that no beam can be injected. In such cases, the vacuum system has to be re-opened to cure the problem. Macroscopic particles such as "dust" degrade the beam lifetime in some electron machines in an unpredictable way. Finding the origin of the problem and its cure is a very difficult job.

9. CONCLUSION

There is a wide range of technical details that have to be considered by the vacuum designers. Whatever solutions are selected they have to allow correct operation of the machine. Thus vacuum design of today's accelerators is a challenging task.

ACKNOWLEDGEMENT

L. Schulz[*], J. Feikes and S. Khan from BESSY are thanked for helpful suggestions, comments and providing figures for the preparation of this paper.

([*] present address: PSI, Villigen, Switzerland)

REFERENCES

[1] A. Liénard, L'Éclairage Électrique, 16 (1898) 5.

[2] J. Larmor, Phil. Mag. 5 (1897) 503.

[3] D. Iwanenko et. al., Phys. Rev. 65 (1944) 343.

[4] J.P. Blewett, Phys. Rev. 69 (1946) 87.

[5] F.R. Elder, Phys. Rev. 71 (1947) 829.

[6] J. Schwinger, Phys. Rev. 75 (1949) 1912.

[7] J.D. Jackson, Classical Electrodynamics, John Wiley & Sons, New York (1962).

[8] K. Hübner, CAS 1989, CERN 90-03 (1990) 24.

[9] R.P. Walker in CAS 1992, CERN 94-01 (1994) 437.

[10] A.G. Mathewson, CAS 1992, CERN 94-01 (1994) 717.

[11] O. Gröbner et al., EPAC, Berlin (1992) 132.

[12] O. Gröbner et al., Vacuum 33 (1983) 397.

[13] H.J. Halama et al., Vacuum 42 (3) (1991) 185.

[14] C. Herbeaux et al., LURE RT/97-03 (1997).

[15] V. Anashin et al, EPAC 98 (Stockholm) 2163.

[16] A.I. Ivanenko et al., EPAC London (1994) 2523.

[17] M. Nordby, EPAC, London (1994) 2515.

[18] A. Poncet, CERN, program Pressure Distribution 2.β; http://www.cern.ch.

[19] R. Kersevan, Cornell University, program MOLFLOW.

[20] J. LeDuff, Nucl. Instr. Meth. A239 (1985) 83.

[21] A. Wrulich, CAS 1992, CERN 94-01 (1994) 409.

[22] J. Haissinski, Thesis, LAL, Orsay (1965).

[23] H.A. Bethe et. al., Proc. R. Soc. A146 (1934) 83.

[24] C. Bernardini et. al., Phys. Rev. Lett. 10 (1963).

[25] H. Bruck, Accélérateurs Circulaires de Particles, Presse Universitaires de France, Paris (1966) and translation into English LANL, LA-TR-72-10 Rev. (1972).

[26] H. Bizek, PAC, Vancouver (1997) 1496.

[27] S. Khan, EPAC, London (1994) 1192.

[28] M.S. Zisman et. al., ZAP Users's Manual, LBL-21270 UC-28 (1986).

[29] A. Piwinski, Proc. of the Int. Conf. on High Energy Acc. (1974) 105.

[30] M. Martini, CERN PS/AA/84-7 and CERN PS/AA/84-9 (1984).

[31] A. Chao, Physics of Collective Beam Instabilities in High Energy Accelerators, John Wiley & Sons, New York (1993).

[32] J.L. Laclare, CAS 1992, CERN 94-01 (1994) 385.

[33] N. Nakamura et. al., PAC, Vancouver (1997) 1756.

[34] MAFIA User's Guide, CST, Darmstadt.

[35] T. Weiland, IEEE Trans. Nucl. Sci., NS-32 (1985) 2738.

[36] S. Khan, PAC, Vancouver (1997) 1703.